Eur Biophys J (2008) 37:183–195
DOI 10.1007/s00249-007-0215-6

ORIGINAL PAPER

Membrane property abnormalities in simulated cases of mild systematic and severe focal demyelinating neuropathies

Diana Stephanova · Mariya Daskalova

Received: 7 May 2007 / Revised: 27 July 2007 / Accepted: 3 August 2007 / Published online: 5 September 2007

Abstract The investigation of multiple nerve membrane properties by mathematical models has become a new tool to study peripheral neuropathies. In demyelinating neuropathies, the membrane properties such as potentials (intracellular, extracellular, electrotonic) and indices of axonal excitability (strength-duration time constants, rheobases and recovery cycles) can now be measured at the peripheral nerves. This study provides numerical simulations of the membrane properties of human motor nerve fibre in cases of internodal, paranodal and simultaneously of paranodal internodal demyelinations, each of them mild systematic or severe focal. The computations use our previous multi-layered model of the fibre. The results show that the abnormally greater increase of the hyperpolarizing electrotonus, shorter strength-duration time constants and greater axonal superexcitability in the recovery cycles are the characteristic features of the mildly systematically demyelinated cases. The small decrease of the polarizing electrotonic responses in the demyelinated zone in turn leads to a compensatory small increase of these responses outside the demyelinated zone of all severely focally demyelinated cases. The paper summarizes the insights gained from these modeling studies on the membrane property abnormalities underlying the variation in clinical symptoms of demyelination in Charcot-Marie-Tooth disease type 1A, chronic inflammatory demyelinating polyneuropathy, Guillain-Barré syndrome and multifocal motor neuropathy. The model used provides an objective study of the mechanisms of these diseases which up till now have not been sufficiently well understood, because quite different assumptions have been given in the literature for the interpretation of the membrane property abnormalities obtained in hereditary, chronic and acquired demyelinating neuropathies.

Keywords Demyelinating neuropathies · Potentials · Excitability properties · Computational neuroscience

Abbreviations

ISD	Internodal systematic demyelination
PSD	Paranodal systematic demyelination
PISD	Paranodal internodal systematic demyelination
IFD	Internodal focal demyelination
PFD	Paranodal focal demyelination
PIFD	Paranodal internodal focal demyelination

Introduction

Accuracy in establishing the diagnosis in nerve disorders is related, in part, to the appropriate application of electrodiagnostic techniques. In routine diagnostic studies, only latency or conduction velocity can be measured accurately. However, while such measurements may be very useful in defining pathology, they provide little insight into underlying disease mechanisms. Moreover, a number of morphological and functional changes such as demyelination, remyelination, branching, axonal tapering, axonal attenuation, cooling, axonal hyperpolarization or depolarization can affect the latency and conduction velocity.

In the 1990s, a non-invasive threshold tracking technique has been developed (Bostock and Baker 1988; Bostock et al. 1998; Kiernan et al. 2000) to study multiple excitability measurements (threshold electrotonus, strength-duration relationship and recovery cycle) in control groups and patients with demyelinating neuropathies such as

D. Stephanova (✉) · M. Daskalova
Institute of Biophysics, Bulgarian Academy of Sciences,
Acad. G. Bontchev Str., Bl. 21, Sofia 1113, Bulgaria
e-mail: dsteph@shiva.bio.bas.bg

Charcot-Marie-Tooth disease type 1A (CMT1A), chronic inflammatory demyelinating polyneuropathy (CIDP), Guillain-Barré syndrome (GBS) and multifocal motor neuropathy (MMN) (Cappelen-Smith et al. 2001; Kaji 2003; Kuwabara et al. 2002, 2003; Nodera et al. 2004; Nodera and Kaji 2006; Priori et al. 2005; Sung et al. 2004). CMT1A is the most common form of hereditary neuropathy and its hallmark is uniform demyelination (Birouk et al. 1997; Dyck et al. 1993). CIDP is one of several chronic demyelinating neuropathies that can occur with other systemic diseases (Barohn et al. 1989; Gorson et al. 2000; Katz et al. 2000). Acute segmental conduction slowing or conduction block in certain parts of the nerve characterizes demyelinating forms of GBS. The latter is classified into acute inflammatory demyelinating polyneuropathy (AIDP) and acute motor axonal neuropathy (AMAN) by electrodiagnostic and pathological criteria (Choudhury and Arora 2001; Feasby et al. 1986; Griffin et al. 1995). Diagnostic features in the MMN are the demonstration of conduction block (Kaji 2003; Priori et al. 2005) or conduction slowing (Delmont et al. 2006). The authors (Bostock 2006; Bostock et al. 1991, 1998; Nodera et al. 2004) also use a computer program based on a two-component (node + internode) model of human motor nerve fibre in order to match the multiple nerve excitability recordings and to provide them with a simple interpretation. However, that model ignores spatial gradients of potential and currents within internodes and cannot propagate intracellular potentials.

Recently, a double cable model (Blight 1985; Halter and Clark 1991; Stephanova and Bostock 1995, 1996) is used to provide an objective interpretation of the membrane property abnormalities obtained in the above discussed demyelinating neuropathies (Stephanova and Alexandrov 2006; Stephanova and Daskalova 2005a, b; Stephanova et al. 2005, 2006a, b, 2007). The following changes have been simulated in these papers: (1) uniform reduction of myelin thickness in all internodes (Stephanova et al. 2005) termed internodal systematic demyelination (ISD); (2) demyelination of all paranodal regions (Stephanova and Daskalova 2005a) termed paranodal systematic demyelination (PSD); (3) simultaneous reduction of myelin thickness and paranodal demyelination in all internodes (Stephanova and Daskalova 2005b) termed paranodal internodal systematic demyelination (PISD); (4) reduction of myelin thickness of up to three internodes (Stephanova et al. 2006a, b) termed internodal focal demyelination (IFD) and (5) simultaneous reduction of myelin thickness and paranodal demyelination of up to three internodes (Stephanova et al. 2007) termed paranodal internodal focal demyelination (PIFD). In the studies, the membrane properties are investigated for three progressively greater degrees (25, 50 and 70%) of demyelination in the systematically demyelinated cases. The same abnormalities are investigated for two progressively greater degrees (70 and 96%) of demyelination in one, two and three consecutive internodes for the focally demyelinated cases. Moreover, the multiple potentials and indices of axonal excitability are compared for mild (70%) systematic and focal demyelinations (Stephanova and Alexandrov 2006). The results show that the membrane properties of these fibres are not identical and depend on the type and degree of demyelination. Each of the above discussed type and degree of demyelination could be realized and observed in patients with motor demyelinating neuropathies (Cappelen-Smith et al. 2001; Kaji 2003; Kuwabara et al. 2002, 2003; Nodera et al. 2004; Nodera and Kaji 2006; Priori et al. 2005; Sung et al. 2004).

The aim of the present study is the simulation of systematically (ISD, PSD, PISD) and focally (IFD, PFD, PIFD) demyelinated cases, using a multi-layered model of human motor nerve fibre (Stephanova 2001) (Paranodal demyelination of up to a given number of internodes is termed paranodal focal demyelination (PFD)). The investigations are performed for myelin reduction values of 70% (in the ISD, PSD, PISD cases) and 96% (in the IFD, PFD and PIFD cases). The first value is not sufficient to develop a conduction block, but the second leads to a block and the corresponding demyelinations are regarded as mild and severe, respectively. Comparison and analysis are also made of the membrane property abnormalities obtained of these mildly systematically and severely focally demyelinated cases. The demyelination is restricted to only three (8th, 9th and 10th) consecutive internodes in all focally demyelinated cases.

Methods

Multi-layered model

Electrical behavior of human studies continues to reveal more information regarding the complex anatomical and diverse electrophysiological properties of myelinated fibres. The electrogenesis of human motor nerve fibre can now be studied successfully using a multi-layered model of this fibre (Stephanova 2001). The myelin sheath as a series of interconnecting parallel lamellae was first presented in the literature in this model, which is a further development of our previous detailed double cable model (Stephanova and Bostock 1995, 1996). The interested reader is referred to the first figure of Stephanova (2001) for an electric equivalent circuit representation of the human motor nerve fibre in which the myelin sheath comprises alternate lipid and aqueous layers. The aqueous layers within the myelin provide appreciable longitudinal and radial conductance, the latter via a spiral pathway. In the cited paper, Kirchoff's current law is used to derive a system of partial differential equations for the electric equivalent circuit. The myelin

sheath is simulated by $N = 150$ interconnected parallel lamellae, and their double structure is simulated by alternating $N = 150$ aqueous and $N = 150$ lipid layers. In this model three cases can be explored and they are thoroughly described in the cited paper. In the present study the first case of the model is used. This is the simplest classical case in which the aqueous layers in the myelin sheath are not taken into account and the 150-lamella model is with infinite aqueous-layered longitudinal (R_{aql}) and radial (R_{aqr}) myelin resistances. The effect of the aqueous layers on the membrane properties of the demyelinated cases will be investigated in our next studies. In the present study, the model assumes a leakage pathway to the internodal axolemma via the paranodal seal resistance and periaxonal space. The R_{pn} (paranodal seal resistance) is 125 MΩ. The entire fibre myelin sheath is characterized by C_{my} (myelin capacitance) 1.5 pF and R_{my} (myelin resistance) 250 MΩ. Each value of the parameters C_{my}, R_{my} for a given spiral differs in arithmetic progression from N. The rule of the arithmetic increasing or decreasing of the value, however, depends on the type of the given parameter and is explicitly written in Stephanova and Alexandrov (2006).

The matched geometry of the complex extended double cable structure to measured morphology of the compartment axonal segments and multi-layered myelin sheath is thoroughly described and discussed in Stephanova (2001). The model fibre comprises 30 nodes and 29 internodes. Each internode is divided into two paranodal and five internodal segments. Non-uniform spatial step sizes are used in accordance with the complex structure of the fibre. These step sizes are defined as the lengths of the consecutive nodal, paranodal and internodal segments. They do not change during the course of the computation. The relatively complicated geometry of the myelin attachment region of the paranode is simulated by a single segment, which joins each internode to the adjacent nodes of Ranvier. The lengths of node, paranode and nodal center to nodal center are 1.5, 200 and 1,400 μm, respectively. Each internodal segment is one fifth of the overall internodal length (998.5 μm). All calculations are carried out for fibres with an axon diameter of 12.5 μm. This axon diameter and the other geometric parameters are the same as those used in most subsequent models of myelinated fibres (Blight 1985; Halter and Clark 1991), i.e., nodal diameter 5 μm, nodal area 24 μm^2, periodicity of myelin lamella 16 nm and myelin thickness 2.4 μm. The temperature is 37°C.

The equations describing the current kinetics of the channels in the multi-layered model are the same as in the double cable model (Stephanova and Bostock 1995, 1996) and are taken from the two-component (node + internode) model of human myelinated motor nerve axons (Bostock et al. 1991). In the latter paper, the thoroughly described and discussed combination of an accurate representation of the ion channels at the node and internode is based on experimental studies of human, rabbit and rat nerves at 37°C. Some of their channel permeabilities according to constant field theory, rather than conductances, have been slightly changed and adjusted (Stephanova and Mileva 2000) to match both the recordings of threshold electrotonus from Bostock et al. (1991, 1994) and the recordings of action potentials in human motor nerves (Dioszeghy and Stålberg 1992). Moreover, the model maximal amplitude, duration and afterpotential of the intracellular potential as well as the kinetics of the nodal sodium current match those of the action potential and sodium channel current as measured in a node of Ranvier of single human myelinated nerve fibre (Schwarz et al. 1995). The channel types and maximum permeabilities (cm^3 s^{-1} × 10^{-9}) are as follows: node, Na (sodium) 9, K_f (fast potassium) 0.07, K_s (slow potassium) 0.26; internode, Na* (sodium) 80, K_f^* (fast potassium) 27, K_s^* (slow potassium) 2, IR* (inward rectifier) 0.008, L_k^* (leak) 0.0064; I^*_{pump} (net outward current generated by electrogenic Na^+/K^+ pump) 0.1 nA; ion concentrations (mM): $[Na^+]_i$ 9, $[Na^+]_o$ 144.2, $[K^+]_i$ 155, $[K^+]_o$ 3. The presented maximum permeabilities of the channel types P_{Na} 9; P_{Kf} 0.07, 27*; P_{Ks} 0.26; P_{IR} 0.008* are the updated ones taken from the paper of Stephanova and Mileva (2000). The * denotes an internodal quantity. (The absolute channel permeabilities (cm^3 s^{-1}) are formed by the multiplication of the channel axolemmal specific permeabilities (cm s^{-1}) by the surface axolemmal areas (cm^2) of the node or internode, respectively, in dependence of the given channel types. The permeability dimension (cm^3 s^{-1}) avoids the current densities). The other membrane parameter values for the normal motor fibre are the same as described earlier (Stephanova and Bostock 1995), i.e., C_n (nodal capacitance) 1 pF, C_i (internodal axolemmal capacitance) 350 pF, R_{ax} (axoplasmic resistance) 8 MΩ, R_{pa} (periaxonal resistance) 300 MΩ, V_r (nodal resting potential) −86.7 mV, V_{ra} (internodal axolemmal resting potential) −86 mV. The full system of differential equations is solved by an implicit numerical integration method (Euler version with subcycles). In this Euler version, a time step usually of 0.001 ms can be automatically halved (when the membrane potential is out of range) during the course of the calculation and the course is repeated at the beginning until the numerical stability of the solution is achieved.

The same multi-layered model is used in the present study to simulate internodal, paranodal and paranodal internodal demyelinations, each of them systematic or focal. The demyelinations are associated with a corresponding loosing or lifting of the myelin end bulbs and myelin lamellae away from the axolemma (Fig. 1). In the figure, the 70% reduction of the myelin lamellae or of the paranodal seal resistance or simultaneously of the paranodal seal resistance and myelin lamellae is uniform along the fibre length

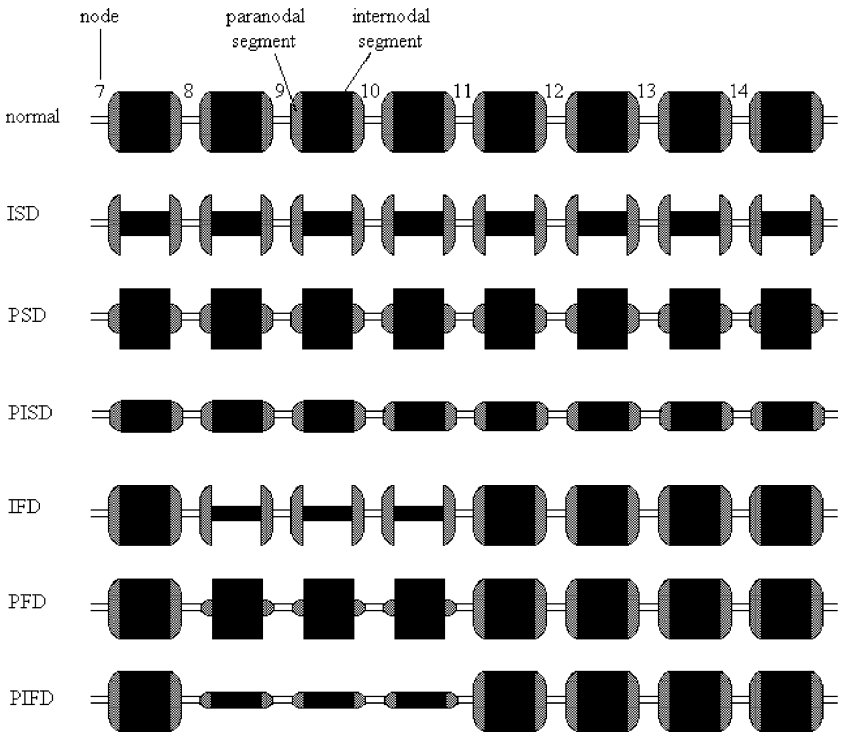

Fig. 1 Schematic diagram of human motor nerve fibres from the 7th to the 14th nodes in the normal, mildly systematically and severely focally demyelinated cases. The 70% reduction of the myelin thickness (ISD) or of the paranodal regions (PSD) or simultaneously of the paranodal regions and myelin thickness (PISD) is uniform along the fibre length of the systematically demyelinated subtypes. The 96% reduction of the same myelin parameters is restricted to only three (8th, 9th and 10th) consecutive internodes for the focally demyelinated subtypes (IFD, PFD, PIFD)

for the systematically demyelinated subtypes. This reduction value is not sufficient to develop a conduction block in the systematically demyelinated subtypes. The 96% reduction of the same myelin parameters is used but restricted to only three (8th, 9th and 10th) consecutive internodes for the focally demyelinated subtypes. This reduction value is not chosen arbitrarily. It is the first degree of the focally demyelinated subtypes for achieving the conduction block in a single internode. Our unpublished data also show that for the systematic demyelinations, the conduction block is achieved when the myelin reduction value is 93% for the ISD, 89% for the PSD and 82% for the PISD. In all calculations, same axonal diameter (12.5 μm) is used which gives possibility for the different demyelinated subtypes to be compared and analyzed. However, both the myelin thickness and external diameter are reduced in the ISD, PISD, IFD, and PIFD cases.

Stimulations, extracellular and electrotonic potentials

To make accurate inference about the anatomical structures or physiological mechanisms involved in electric stimulation, one must know which elements are stimulated. Two cases of fibre stimulation are considered. The stimulation for producing intracellular potentials is simulated by adding a short (0.1 ms) rectangular current pulse to the center of the first node. This case of point application of current intra-axonally at the center of the node closely approximates the effects of point application of current extra-axonally at the node and realizes a point fibre polarization. The intracellular potentials in the case of adaptation (i.e., in the case of intracellular current application delivered simultaneously at the center of each internodal segment) are simulated by adding a long-lasting suprathreshold depolarizing pulse. This second case closely approximates the effects of external surface stimulation with a large electrode and realizes a periodic kind of uniform fibre polarization. The generated intracellular potentials, in the second case of fibre stimulation, are then used as input to a line source model (Stephanova et al. 1989) that allows calculation of the corresponding extracellular potentials at various radial distances in the surrounding volume conductor. The extracellular recordings provide information about the bioelectric activity of a specific region of tissue. In that sense, the description of the extracellular potential field of a single fibre in an extensive conducting media is of great interest in the field of electrophysiology. The extracellular potentials of the normal human motor nerve fibre, calculated by us, are in the same ranges as reported in the literature (Ganapathy and Clark 1987; Schoonhoven and Stegeman 1995). The relationship between the extracellular potentials from volume conductor model simulations and recorded compound nerve action potentials is thoroughly discussed in the critical review by Schoonhoven and Stegeman (1995). The line source model is the most frequently used model in the literature for calculation of the extracellular potentials (Ganapathy and Clark 1987; Schoonhoven and Stegeman 1995; Stegeman et al. 1979).

The electrotonic potentials are simulated by adding a 100 ms subthreshold current to the center of each internodal

segment and the case of periodic kind of uniform fibre polarization is also realized. The periodic kind of uniform polarization is first simulated in the human motor electrotonus model (Stephanova and Bostock 1996). The potentials are calculated for polarizing currents, which correspond to 0.4 times the threshold for a 1 ms current pulse.

Excitability calculations

The indices of the axonal excitability (such as strength-duration, charge-duration curves, strength-duration time constants, rheobases and recovery cycles) delivered from single or pairs of threshold stimuli are investigated in the case of adaptation. The threshold stimulus duration is increased in 0.025 ms steps from 0.025 ms to 1 ms, to obtain the strength-duration curves. According to the classical theory, the strength-duration time constant (chronaxie) of an excitable structure is based on the single passive (RC) membrane parameters in parallel and can be calculated by the classical Weiss's formula (Weiss 1901) applied to the linear charge-duration curve. In the human myelinated nerve fibre, RC parameters in parallel are as in the nodal and internodal axolemma as well as in the myelin sheath. Because of this complicated situation, the strength-duration curves of the normal and demyelinated fibres are not natural exponential expressions and the charge-duration curves are not linear. In this case a polynomial function of degree 2 (transfer standard parabola), which relates threshold charge (Q) to stimulus duration (t), provides an accurate fit of the data: $Q = a_2[t^2 + (a_1/a_2)\times t + a_0/a_2]$, where a_0, a_1, a_2 are the polynomial coefficients. The strength-duration time constant is defined as the absolute value of the smallest square root of the function (i.e., only one of both direct intercepts of the regression curve on the duration axis has a biophysical sense and only this direct intercept is shown on the below given figures). The rheobasic current is defined as the final decreased threshold value, after which the potential generation cannot be obtained with an increase of the stimulus duration.

When two equal-duration pulses are used in pairs, the response of the second (testing) pulse in the refractory period may be greater or less than the response of the first (conditioning) pulse and depends on the conditioning-test intervals. To obtain the time course of recovery of the axonal excitability following a single threshold stimulus (the recovery cycle), test stimuli of 1.0 ms duration are delivered at conditioning-test intervals of 2–100 ms after a threshold conditioning stimulus of 1.0 ms duration. The recovery cycle depends on the regenerative depolarization caused by the conditioning potential and can be explained by the delay-dependent testing potential. During the absolute refractory period when the inactivation of Na^+ channels is high and the activation of K^+ channels is low, the threshold potential (Vt) and the corresponding threshold current for the testing pulse are increased due to the more expressed increase of the critical membrane potential (Ec). ((Vt = Ec − Er); Er is resting membrane potential). With increasing the conditioning-test interval, Ec is decreased and as the membrane potential remains above the Er, the threshold potential becomes lower than that of the initial one. The result is the change from subnormality to supernormality of the membrane excitability.

We would like to note that although the calculations for the 70% systematic demyelination are done with our new multi-layered model, the results of the model approximation used here show that they are almost identical with those from our paper (Stephanova and Alexandrov 2006). Although the results for this reduction value are presented here in a different manner than in the cited paper, permission has been granted from the original journal for the use of these figures.

Results

Intracellular, electrotonic and extracellular potentials

A comparison of the temporal intracellular potentials is presented for the normal, ISD, PSD, PISD (Fig. 2a) and IFD, PFD, PIFD (Fig. 2b) cases of human motor nerve fibres. The potentials are at each node, from the 7th to the 14th. They are of constant amplitude at the successive nodes for a given systematic demyelination (Fig. 2a). Compared to the normal case, the potentials have lower peak amplitudes. The afterpotential amplitudes are larger. Node-to-node conduction is slower. The conduction velocities, calculated from the times of the potential maxima at the nodes are 58, 31, 45 and 25 m/s for the normal, ISD, PSD and PISD cases, respectively. The maximal amplitudes are 38, 18, 21 and 9 mV for the same cases, respectively. The progressively greater increase in focal loss of myelin blocks the invasion of the potentials into the demyelinated zone (Fig. 2b). Thus, with the increase of the demyelinated subtype from the IFD to the PIFD, the conduction failure occurs more rapidly.

The electrotonic potentials are also compared for the normal, ISD, PSD, PISD (Fig. 3a) and IFD, PFD, PIFD (Fig. 3b) cases of the fibres. The temporal distributions of the potentials during and after 100 ms depolarizing and hyperpolarizing currents (±40% of threshold) are again at each node, from the 7th to the 14th. However, because of the systematic demyelination (Fig. 3a), each node behaves identically, and an overlap of the potentials at the nodes is obtained. The same is also valid for the normal case. There are small differences in the potentials during and after the 100 ms depolarizing and hyperpolarizing currents between

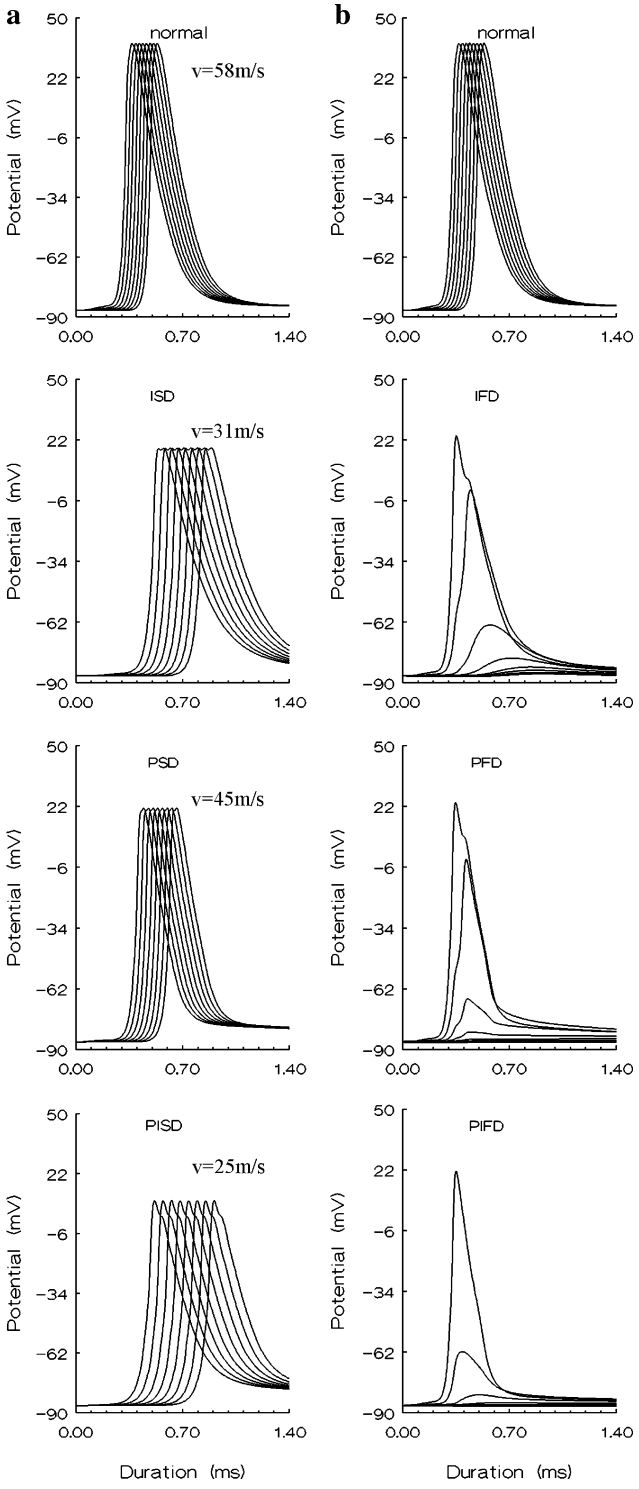

Fig. 2 Comparison of the intracellular potentials of human motor fibres in the normal, ISD, PSD, PISD (**a**) and IFD, PFD, PIFD (**b**) cases. The normal case in the first row is repeated for a better comparison. The potentials in response to 0.1 ms threshold current pulses are presented at each node from the 7th to the 14th. The focal cases are characterized with three (8th, 9th and 10th) consecutively demyelinated internodes. The 70% reduction value is not sufficient to develop conduction block in all investigated systematic demyelinations, which are regarded as mild. The 96% reduction value leads to a block and the corresponding focal demyelinations are regarded as severe. The conduction velocities are added to the left of each data row

the normal and ISD cases. When the normal case is compared with the PSD and PISD cases, the obtained differences are the abnormally greater increase in the early and late parts of the hyperpolarizing responses. The potentials are the most abnormal in the PISD case. For the focally demyelinated subtypes (Fig. 3b), the depolarizing and hyperpolarizing electrotonic potentials are similar, with a small drop to a minimum amplitude in the 10th node and with a small rise to a maximum amplitude in the 14th node. For the PIFD case, the depolarizing and hyperpolarizing responses show the largest drop to a minimum amplitude in the 10th node and the largest rise to a maximum amplitude in the 14th node, than those for the IFD and PFD cases.

Figure 4 illustrates the temporal distributions of the intracellular potentials (V) and their corresponding extracellular potentials (P) in the case of adaptation for the normal, mildly systematically and severely focally demyelinated cases, respectively. The potentials are at each node, from the 7th to the 14th. However, because of the systematic demyelination, each node again behaves identically, and an overlap of the potentials at the nodes is obtained in Fig. 4a. The potential overlap is also valid for the normal case. The extracellular potential amplitudes depend on the radial distance of the field point for all investigated cases. Close to the fibre membrane ($r = 0.05$ mm), the potentials have a two-phase shape, while far from the membrane at the volume conductor ($r = 1.0$ mm), they have the usual three-phase shape. At large radial distances ($r \geq 5$ mm) the shape of potentials is the same. The potentials in the PSD and PISD cases have increased polyphasia at $r = 1.0$ mm (Fig. 4a). The peak-to-peak amplitude of the potentials decreases in the demyelinated zone of the severely focally demyelinated cases (Fig. 4b), and this can be seen more clearly in Fig. 5. In this figure, the extracellular potential time courses for radial distance $r = 1$ mm are repeated from Fig. 4b. The potentials are plotted for the same eight consecutive nodes from the 7th to the 14th as shown in the first row, except in the second, third, fourth and fifth rows where the potentials are shown at the 7th, 8th, 9th and 10th nodes, respectively. The results show that with the increase of the demyelinated subtype from the IFD to the PIFD, the peak-to-peak amplitude of the potentials abnormally decreases until the potential dies out. However, the potential shapes in the regions distal to the demyelinated zone are normal.

Axonal excitability indices

The strength-duration and charge-duration curves for the normal, mildly systematically (Fig. 6a) and severely

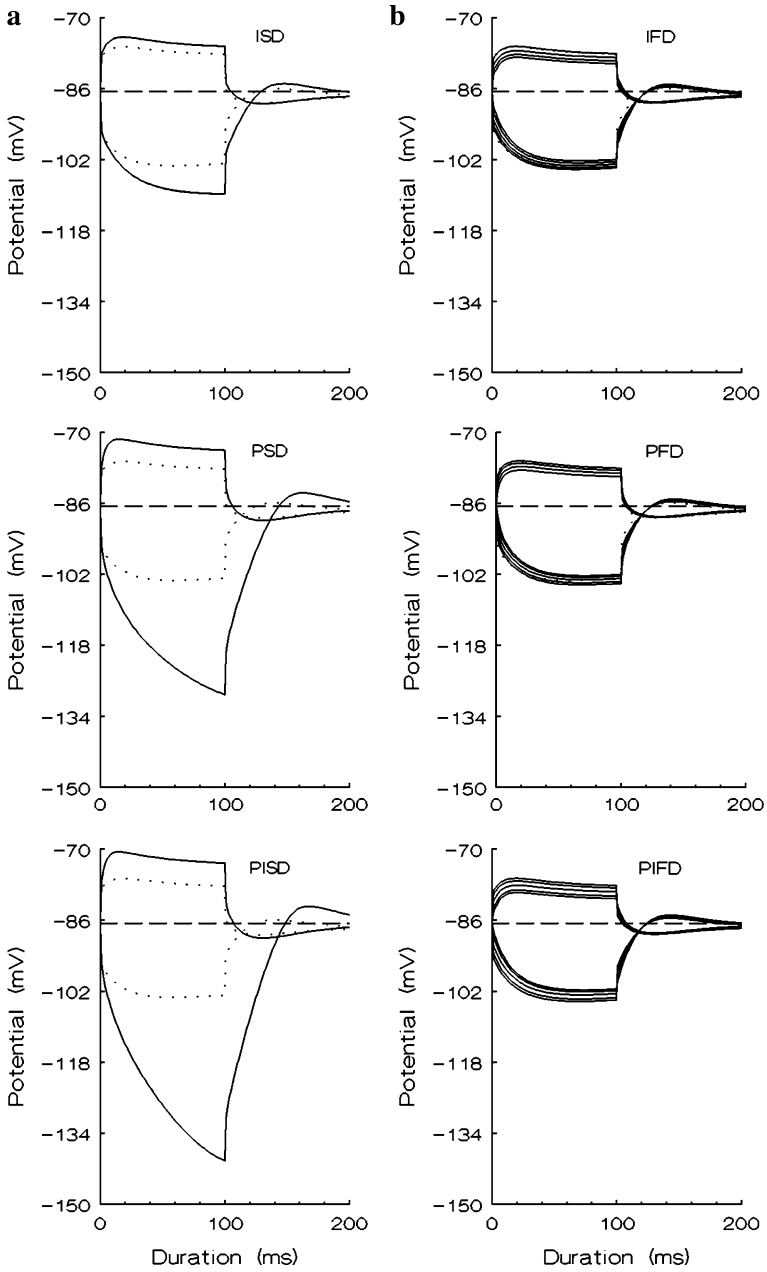

Fig. 3 Comparison of the electrotonic potentials of human motor fibres in the normal (*dotted lines*), ISD, PSD, PISD (**a**) and IFD, PFD, PIFD (**b**) (*continued lines*) cases. The electrotonic potentials in response to 100 ms depolarizing and hyperpolarizing current pulses (±40% of threshold) are presented at each node from the 7th to the 14th

focally (Fig. 6c) demyelinated cases are shown. Histograms are also used to provide a better illustration of the strength-duration time constants and rheobases (Fig. 6b, d). In the different strength-duration curves, the threshold currents are significantly higher in the systematically demyelinated cases than in the normal one. The strength-duration time constant is substantially longer for the ISD case and substantially shorter for the PSD case than for the normal one. There is an inverse relationship between the strength-duration time constants and rheobasic currents for the normal, PSD and PISD cases, but this is not the same for the ISD case. In this case, the strength-duration time constant and rheobasic current are increased. The strength-duration time constants are 0.291, 0.583, 0.092, 0.211 ms and the rheobases are 0.388, 0.568, 0.842, 1.020 nA for the normal, ISD, PSD and PISD cases, respectively. The progressively greater increase in focal loss of myelin slightly increases threshold currents in the cases of severe demyelination (Fig. 6c, d). They are higher in the IFD, PFD and PIFD cases than in the normal one. The strength-duration time constants are shorter. There is an inverse relationship between the strength-duration time constants and rheobases for the normal and abnormal cases. The strength-duration time constants are 0.291, 0.250, 0.236 and 0.235 ms for the normal, IFD, PFD, PIFD cases, respectively. The rheobasic currents are 0.388, 0.431, 0.447 and 0.454 nA, respectively, for the same cases.

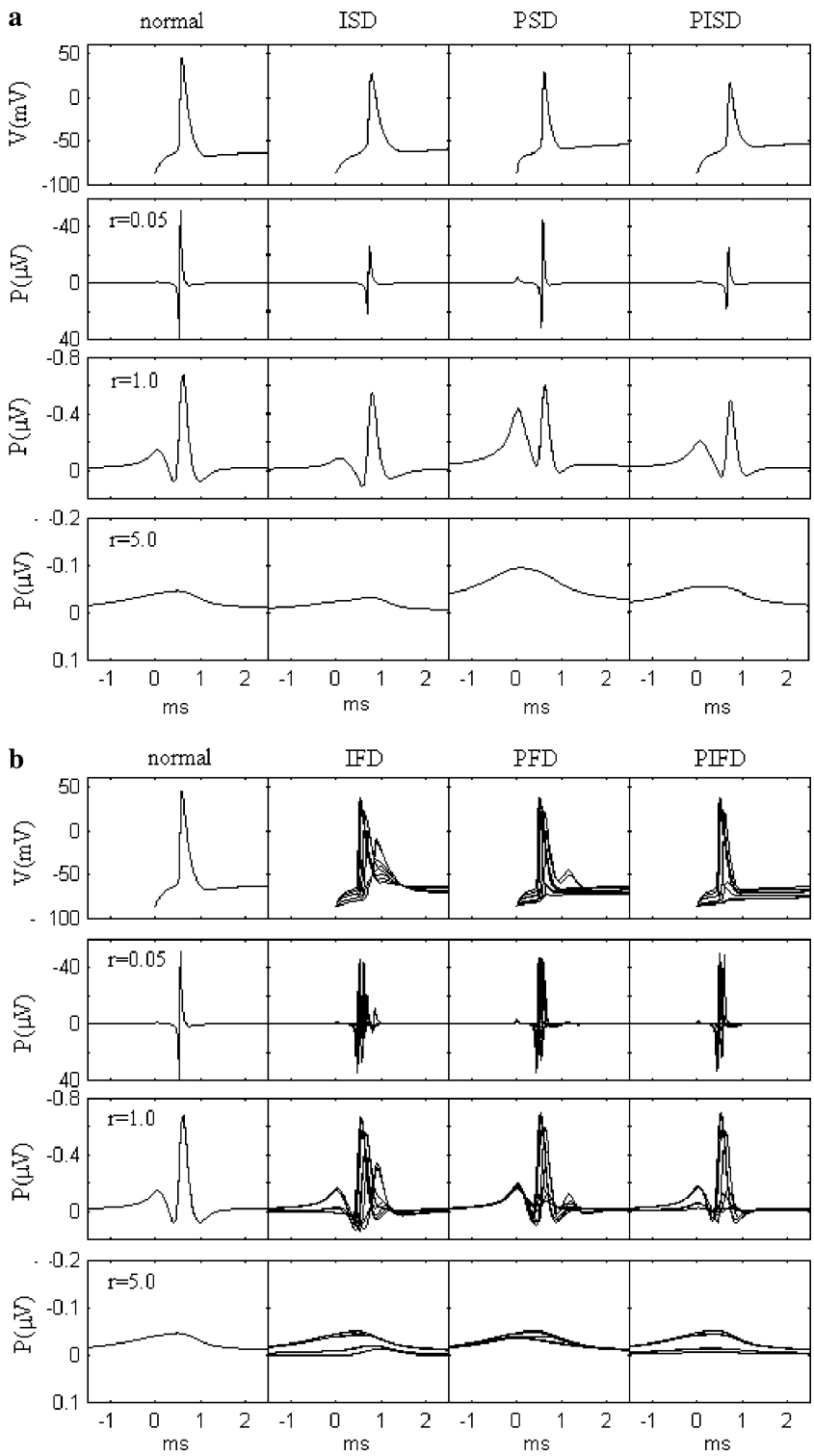

Fig. 4 In the case of adaptation, the temporal intracellular potentials (*V*) and their corresponding extracellular potentials (*P*) are presented in the normal, ISD, PSD, PISD (**a**) and IFD, PFD, PIFD (**b**) cases. The intracellular potentials are simulated by adding long-lasting depolarizing pulses, which correspond to 1.1 times the threshold for a 1 ms current pulse. The potentials are at each node from the 7th to the 14th. The extracellular potentials are given for three radial distances ($r = 0.05$, 1.0 and 5.0 mm). Fig. 4a by permission of JIN (2006) 5:595–623

The excitability changes of the axons in the normal and systematically demyelinated cases during the 100 ms recovery cycles are illustrated in Fig. 7a. The recovery cycles show that the axonal excitability changes in the normal and ISD cases are similar. The axonal types are initially unexcitable, then excitable with a raised threshold and after about 2.5 ms they are superexcitable. In the unexcitable case, the axons are in the absolute refractory period, during which they cannot not generate second potential no matter how strong the testing depolarizing pulses are. Then the axons are in the relative refractory period, during which a stronger than conditioning stimulus is required to generate the second action potential. In the superexcitable case, the testing stimulus generating a second action potential is less than the

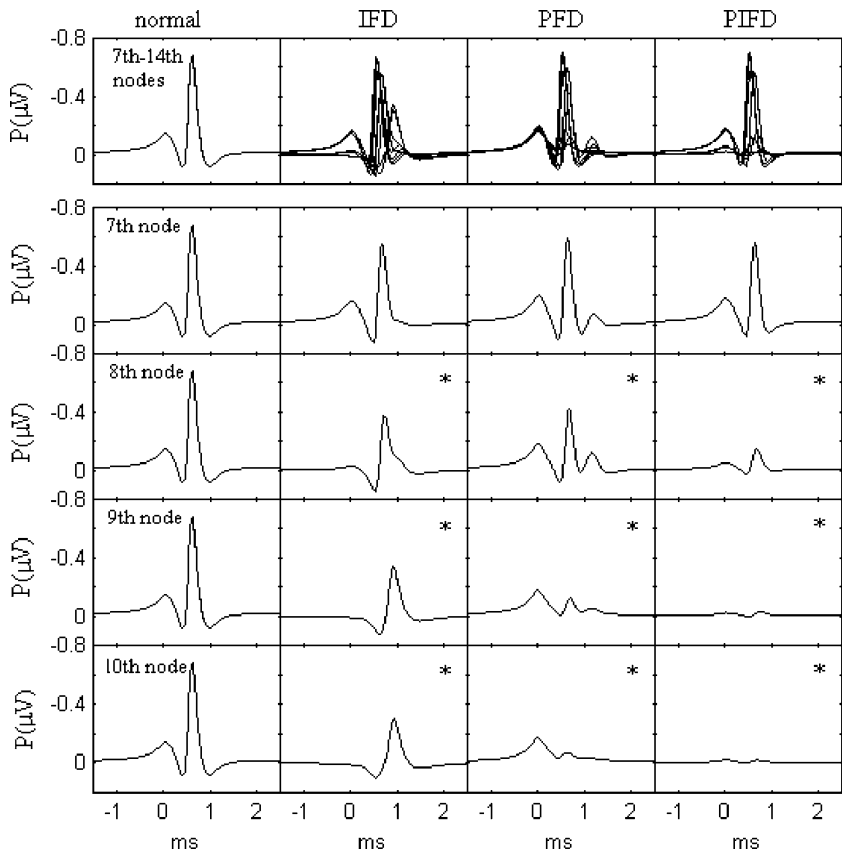

Fig. 5 The extracellular potentials (*P*) in the normal and IFD, PFD, PIFD cases are repeated for the radial distance $r = 1$ mm. The superpositions of potentials are for eight consecutive nodes from the 7th to the 14th as shown in the first row, except in the second, third, fourth, and fifth rows, where the potentials shown are at the 7th, 8th, 9th, and 10th nodes, respectively. * (*columns*) indicates the demyelinated internodes between the given nodes

conditioning stimulus. Superexcitability is usually followed by a late subexcitability. The ISD axon has greater refractoriness, superexcitability and less late subexcitability than those for the normal axon. There is an increase in the refractoriness without an increase in the relative refractory period in this demyelinated axon. The recovery cycles show that the axonal excitability changes in the PSD and PISD cases are similar. Both axonal subtypes have abnormally greater superexcitabilities. In these cases compared to the normal one, the recovery cycles are without relative refractory periods and have only superexcitable and subexcitable periods. The same investigations of the axonal excitability changes during the 100 ms recovery cycles are repeated for the IFD, PFD and PIFD cases of the fibres and are illustrated in Fig. 7b. The recovery cycles show that the axonal excitability changes in all focally demyelinated cases are similar. The axons have slightly less refractoriness, greater superexcitability and less late subexcitability than those for the normal axon. However, the recovery cycles are near-overlap for the PFD and PIFD cases.

Discussion

This study shows a number of differences in the membrane properties between the simulated mildly systematically and severely focally demyelinated fibers. The uniformly reduced amplitudes, prolonged duration and slowed conduction velocities of the intracellular potentials are characteristic for the investigated systematically demyelinated subtypes. The conduction block is typical for the severely focally demyelinated fibers. The intracellular potential changes in demyelinated fibers are determined by the kinetics of the nodal ion currents. The kinetics of the ion currents passing through paranodally or internodally demyelinated fibers is thoroughly discussed in our previous papers (Stephanova and Chobanova 1997; Stephanova and Kossev 1997). In these papers, the current kinetics shows that the reduced conduction obtained in the paranodally demyelinated fibers is due to the decrease of the external membrane current and the limitation for the paranodally short-circuited current to pass longitudinally to the periaxonal space. The same explanation is valid for the PSD and PFD cases investigated here. According to the cited papers, the reduced conduction obtained in the internodally demyelinated fibers is due to the increase in the transmyelin current generation and the limitation for the externally recorded nodal current to pass longitudinally via the paranodal seal resistance to the periaxonal space. The same explanation is valid for the ISD and IFD cases investigated here. Compared to the ISD, PSD, IFD and PFD cases, the simulated PISD and PIFD cases show qualitatively very

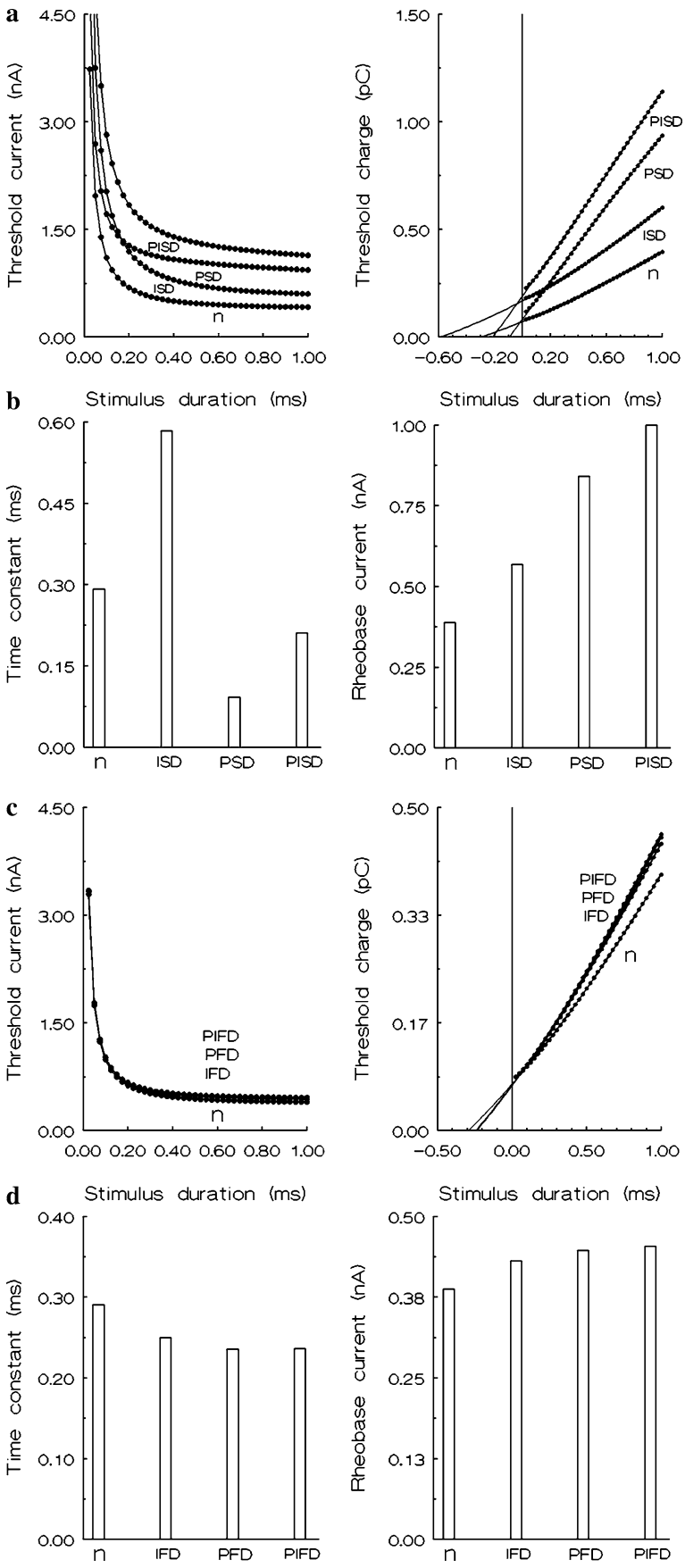

Fig. 6 Comparison between the strength-duration curves, charge-duration curves, strength-duration time constants and rheobasic currents in the normal, ISD, PSD, PISD (**a**, **b**) and IFD, PFD, PIFD (**c**, **d**) cases. Fig. 6 parts of a, b by permission of JIN 2006 5:595–623

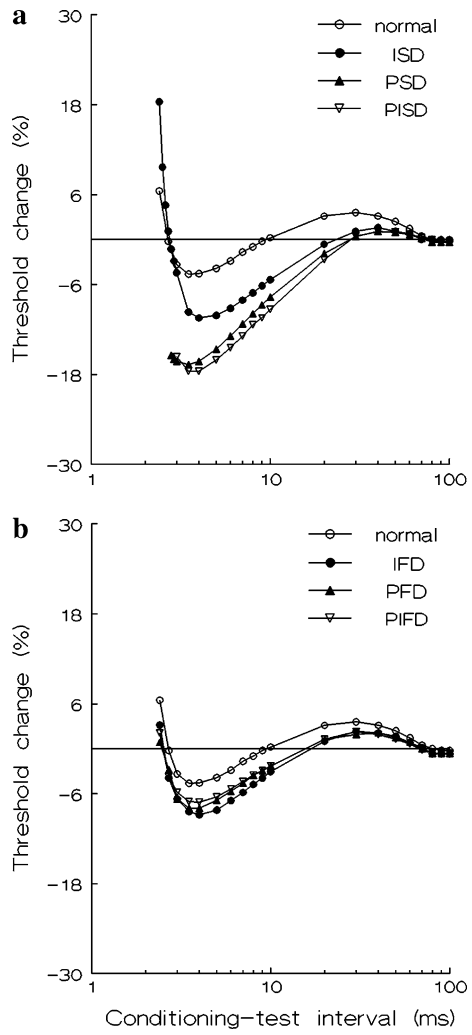

Fig. 7 Comparison of the recovery cycles in the normal, ISD, PSD, PISD (**a**) and IFD, PFD, PIFD (**b**) cases of human motor nerve fibres. For all investigated cases, the *y*-axis is defined as $100 \times (I_{test} - I_{cond})/I_{cond}$ (%), where I_{test} (nA) and I_{cond} (nA) are the threshold currents of the testing and conditioning pulses, respectively. Fig. 7a by permission of JIN (2006) 5:595–623

similar changes of the potentials. Consequently, the effect of reduced myelin lamellae, additionally increased by reduced paranodal seal resistance, is consistent with the reduced conduction obtained in the investigated PISD and PIFD cases. The conduction slowing simulated in the ISD, PSD and PISD subtypes is a characteristic feature described in demyelinating neuropathies, namely CMT1A, CIDP (Cappelen-Smith et al. 2001; Nodera et al. 2004; Sung et al. 2004) and *n*-hexane neuropathy (Chang et al. 1998; Kuwabara et al. 1993). Conduction block is a critical diagnostic feature in GBS and MMN patients (Kaji 2003; Priori et al. 2005).

The electrotonic potentials allow the accommodative responses to polarizing currents to be investigated. The kinetics of the ionic currents defining the electrotonic potentials (Stephanova and Alexandrov 2006; Stephanova and Bostock 1996) show that the slow components of electrotonic, transaxonal, and transmyelin potentials depend on the activation of the channel types in the nodal or internodal axolemma, whereas the fast components of the potentials are determined mainly by the passive cable responses, i.e., by the capacitances and resistances of the corresponding different segments along the fiber. In the cited paper, it is shown that for the hyperpolarizing pulses, the contribution of the activating inward rectifier (IR) channels dominates in the total ionic currents passing through the paranodal and internodal segments. For the depolarizing pulses, the contribution of the activating potassium (K^+) channels dominates in the total ionic currents passing through the corresponding different segments along the fiber. Furthermore, the depolarizing electrotonic potential in the nodes is determined mainly by the activation of the slow potassium channels and the other channels as sodium (Na^+) and fast potassium has a minor contribution to its generation. Our results show that there are no significant differences between the normal and ISD cases in the accommodated responses to prolonged subthreshold depolarizing and hyperpolarizing currents. However, these responses in the PSD and PISD cases are abnormally greater to the hyperpolarizing currents than in the normal case. The greater hyperpolarizing potentials show that, for the axons studied, the behavior of internodal accommodative permeabilities is largely affected by the demyelinating pathology. The simulated electrotonic potentials in the ISD case are rather similar to those described in demyelinating neuropathies, namely CMT1A (Nodera et al. 2004; Nodera and Kaji 2006), whereas, the potentials in the PSD and PISD cases are similar to those described in subgroups of CIDP (Nodera and Kaji 2006; Sung et al. 2004).

Our results also show that there is a decrease in the electrotonic responses to subthreshold polarizing currents in the focally demyelinated cases. The same results are obtained for AIDP patients who tend to have the smaller slow phase of threshold change to polarizing currents than normal subjects (Kuwabara et al. 2002). Our previous results (Stephanova and Alexandrov 2006; Stephanova et al. 2006a, b) confirm that mild (70%) focal demyelination, not sufficient to develop conduction block, does not significantly affect electrotonic, extracellular potentials, strength-duration time constants, rheobases, and recovery cycles. Their values are equal to or near normal values.

The extracellular potentials in the PSD, PISD, PFD and PIFD cases have increased polyphasia, which is a characteristic feature of compound motor action potentials (CMAPs) in patients with demyelinating neuropathies (Donofrio and Albers 1990).

The strength-duration time constants are longer in the ISD case and shorter in the PSD and PISD cases than in the

normal one. However, they are slightly shorter in the IFD, PFD and PIFD cases. These relationships are attributed to the current thresholds as they can be seen in the strength-duration curves for the corresponding cases. Longer and shorter time constants are characteristic for CMT1A (Nodera et al. 2004; Nodera and Kaji 2006) and CIDP (Cappelen-Smith et al. 2001; Nodera and Kaji 2006) patients, respectively. The slightly shorter time constants are characteristics for the demyelinating forms of GBS.

Moreover, the pattern of the recovery cycles for the PSD and PISD cases is characteristic for CIDP patients (Sung et al. 2004), whereas the recovery cycles for the IFD, PFD and PIFD are characteristic for the median motor nerves in AIDP patients (Kuwabara et al. 2002; Nodera and Kaji 2006).

In summary, the current study indicates quite different abnormalities in the potentials and axonal excitability indices of mild systematic and severe focal demyelinations of human motor nerve fibres. The changes in the excitability properties obtained in these simulations are in good accordance with the data from patients with CMT1A, CIDP, GBS and MMN. Our previous studies show that in the mild focal demyelinations, changes are so slight as to be essentially indistinguishable from normal values (Stephanova and Alexandrov 2006). It was concluded that the excitability-based approaches that have shown strong potential as diagnostic tools in systematically demyelinated conditions may not be useful in detecting mild focal demyelinations. In contrast, the abnormal potentials and excitability indices in severe focal demyelinations are quite different from those in mild systematic demyelinations and can provide important information about the pathophysiology of acquired demyelinating neuropathies. However, compared to mild systematic demyelination, the effect of severe focal demyelination is relatively weak. This can explain the reason for measured minor changes in the threshold electrotonus and for obtaining no significant changes in excitability properties in patients with GBS.

The simulations are done using a well-validated model. It incorporates a double-cable structure, with explicit representation of the nodes of Ranvier, paranodal, internodal sections of the axon and multi-layered myelin sheath. This model is able to reproduce a wide range of experimental data on the potentials and excitability properties in human demyelinating neuropathies. The results show that the systematic demyelinations are specific indicators for hereditary and chronic neuropathies, whereas the focal demyelinations are specific indicators for acquired demyelinating neuropathies. The myelin reduction values, leading to conduction block in the various focally and systematically demyelinated human motor fibres, can be defined by the model. Our previous and present studies confirm that the transition from conduction slowing to conduction block leads to amplification of the degree of the membrane property changes, as the direction of these changes is maintained. The effect of aqueous layers within the myelin on the multiple membrane properties of the various focally and systematically demyelinated cases can also be predicted by this model. The model provides an objective interpretation of the mechanisms of the membrane property abnormalities obtained in the hereditary, chronic and acquired demyelinating neuropathies, which up till now have not been sufficiently well understood. Quite different assumptions have been given in the literature for the membrane property mechanisms of these diseases. For example, in the review by Nodera and Kaji (2006), where a difference between systematic and focal demyelinations has not been made, it is written that: (1) “Given the almost constant membrane capacitance, the major factor determining passive membrane behavior is the resistance of the membrane”; (2) “Therefore, the degree of potassium channel opening determines both membrane conductance (the inverse of resistance) and resistance”; (3) “Depolarization decreases the Na^+ current through the persistent channels, resulting in a lower rheobase, and hyperpolarization has the opposite effect. As the charge–duration relationship suggests, SDTC (strength-duration time constant) behaves in the opposite direction than does the membrane potential, being increased by depolarization and decreased by hyperpolarization”; (4) “Paranodal demyelination increases capacitance and SDTC”, and etc. However, we have to keep in mind that neither model of demyelinated axon looks like an actual demyelinating neuropathy, but they are simple ways of showing the effect of various demyelinations and their degrees on the multiple membrane properties of these neuropathies.

References

Barohn RJ, Kissel JT, Warmolts JR, Mendell JR (1989) Chronic inflammatory demyelinating polyradiculoneuropathy; clinical characteristics, course and recommendations for diagnostic criteria. Arch Neurol 46:878–884

Birouk N, Gouider R, Le Guern E, Gugenheim M, Tardieu S, Maisonobe T, Le Forestier N, Agid Y, Brice A, Bouche P (1997) Charcot-Marie-Tooth disease type 1A with 17p11.2 duplication. Clinical and electrophysiological phenotype study and factors influencing disease severity in 119 cases. Brain 120:813–823

Blight A (1985) Computer simulation of action potentials and afterpotentials in mammalian myelinated axons: the case for a low resistance myelin sheath. Neuroscience 15:13–31

Bostock H (2006) MEMFIT: a computer program to aid interpretation of multiple excitability measurements on human motor axons. Clin Neurophysiol 117:S49–S111

Bostock H, Baker M (1988) Evidence for two types of potassium channels in human motor axons in vivo. Brain Res 462:354–358

Bostock H, Baker M, Reid G (1991) Changes in excitability of human motor axons underlying post-ischaemic fasciculations: evidence for two stable states. J Physiol 441:537–557

Bostock H, Burke D, Hales JP (1994) Differences in behavior of sensory and motor axons following release of ischaemia. Brain 117:225–234

Bostock H, Cikurel K, Burke D (1998) Threshold tracking techniques in the study of human peripheral nerve. Muscle Nerve 21:137–158

Cappelen-Smith C, Kuwabara S, Lin CS, Mogyoros I, Burke D (2001) Membrane properties in chronic inflammatory demyelinating polyneuropathy. Brain 124:2439–2447

Chang AP, England JD, Garcia CA, Summer AJ (1998) Focal conduction block in n-hexane polyneuropathy. Muscle Nerve 21:964–969

Choudhury D, Arora D (2001) Axonal Guillain-Barré syndrome: a critical review. Acta Neurol Scand 103:267–277

Delmont E, Azulay JP, Giorgi R, Attarian S, Verschueren A, Uzenot D, Pouget J (2006) Multifocal motor neuropathy with and without conduction block: a single entity? Neurology 67:592–596

Dioszeghy P, Stålberg E (1992) Changes in motor and sensory nerve conduction parameters with temperature in normal and diseased nerve. Electroencephalogr Clin Neurophysiol 85:229–235

Donofrio PD, Albers JW (1990) Polyneuropathy: classification by nerve conduction studies and electromyography. Muscle Nerve 13:889–903

Dyck PJ, Chance P, Lebo R, Camey AJ (1993) Hereditary motor and sensory neuropathies. In: Dyck PJ, Thomas PK, Griffin JW, Low PA, Poduslo JF (eds) Peripheral neuropathy, 3rd edn, WB Saunders, Philadelphia, pp 1094–1136

Feasby TE, Gilbert JJ, Brown WF, Bolton CF, Hahn AF, Koopman WF, Zochodne DW (1986) An acute axonal form of Guillain-Barré polyneuropathy. Brain 109:1115–1126

Ganapathy L, Clark JW (1987) Extracellular currents and potentials of the active myelinated nerve fibre. Biophys J 52:749–761

Gorson KC, Ropper AH, Adelman LS, Weinberg DH (2000) Influence of diabetes mellitus on chronic inflammatory demyelinating polyneuropathy. Muscle Nerve 23:37–48

Griffin JW, Li CY, Ho TW, Xue P, Macko C, Gao CY, Yang C, Tian M, Mishu B, Cornblath DR (1995) Guillain-Barré syndrome in northern China. The spectrum of neuropathological changes in clinically defined cases. Brain 118:575–595

Halter J, Clark J (1991) A distributed-parameter model of the myelinated nerve fibre. J Theor Biol 148:345–382

Kaji R (2003) Physiology of conduction block in multifocal motor neuropathy and other demyelinating neuropathies. Muscle Nerve 27:285–296

Katz JS, Saperstain DS, Gronseth G, Amato AA, Barohn RJ (2000) Distal acquired demyelinating symmetric neuropathy. Neurology 54:615–620

Kiernan MC, Burke D, Andersen KV, Bostock H (2000) Multiple measures of axonal excitability: a new approach in clinical testing. Muscle Nerve 23:399–409

Kuwabara S, Nakajima M, Tsuboi Y, Hirayama K (1993) Multifocal conduction block in n-hexane neuropathy. Muscle Nerve 16:1416–1417

Kuwabara S, Ogawara K, Sung JY, Mori M, Kanai K, Hattori T, Yuki N, Lin CS, Burke D, Bostock H (2002) Differences in membrane properties of axonal and demyelinating Guillain-Barré syndromes. Ann Neurol 52:180–187

Kuwabara S, Bostock H, Ogawara K, Sung JY, Kanai K, Mori M, Hattori T, Burke D (2003) The refractory period of transmission is impaired in axonal Guillain-Barré syndrome. Muscle Nerve 28:683–689

Nodera H, Kaji R (2006) Nerve excitability testing and its clinical application to neuromuscular diseases. Clin Neurophysiol 117:1902–1916

Nodera H, Bostock H, Kuwabara S, Sakamoto T, Asanuma K, Sung JY, Ogawara K, Hattori N, Hirayama M, Sobue G, Kaji R (2004) Nerve excitability properties in Charcot-Marie-Tooth disease type A1. Brain 27:203–211

Priori A, Bossi B, Ardolino G, Bertolasi L, Carpo M, Nobile-Orazio E, Barbieri S (2005) Pathophysiological heterogeneity of conduction blocks in multifocal motor neuropathy. Brain 128:1642–1648

Schoonhoven R, Stegeman DF (1995) Models and analysis of compound nerve action potentials. Crit Rev Biomed Eng 19:47–111

Schwarz JR, Reid G, Bostock H (1995) Action potentials and membrane currents in the human node of Ranvier. Pflügers Arch 430:283–292

Stegeman DF, de Weerd JPC, Eijkman EG (1979) A volume conductor study of compound action potentials of nerves in situ: the forward problem. Biol Cybern 33:97–111

Stephanova DI (2001) Myelin as longitudinal conductor: a multi-layered model of the myelinated human motor nerve fibre. Biol Cybern 84:301–308

Stephanova DI, Alexandrov AS (2006) Simulated mild systematic and focal demyelinating neuropathies: membrane property abnormalities. J Integr Neurosci 5:595–623

Stephanova DI, Bostock H (1995) A distributed-parameter model of the myelinated human motor nerve fibre: temporal and spatial distributions of action potentials and ionic currents. Biol Cybern 73:275–280

Stephanova DI, Bostock H (1996) A distributed-parameter model of the myelinated human motor nerve fibre: temporal and spatial distributions of electrotonic potentials and ionic currents. Biol Cybern 74:543–547

Stephanova DI, Chobanova M (1997) Action potentials and ionic currents through paranodally demyelinated human motor nerve fibres: computer simulations. Biol Cybern 76:311–314

Stephanova DI, Daskalova M (2005) Differences in potentials and excitability properties in simulated cases of demyelinating neuropathies. Part II. Paranodal demyelination. Clin Neurophysiol 116:1159–1166

Stephanova DI, Daskalova M (2005) Differences in potentials and excitability properties in simulated cases of demyelinating neuropathies. Part III. Paranodal internodal demyelination. Clin Neurophysiol 116:2334–2341

Stephanova D, Kossev A (1997) Action potentials and ionic currents through internodally demyelinated human motor nerve fibres. I. Computer simulations. Comp Rend l'Acad Bulg Sci 50(3):107–110

Stephanova DI, Mileva K (2000) Different effects of blocked potassium channels on action potentials, accommodations, adaptation and anode break excitation in human motor and sensory myelinated nerve fibres: computer simulations. Biol Cybern 83:161–167

Stephanova D, Trayanova N, Gydikov A, Kossev A (1989) Extracellular potentials of a single myelinated nerve fiber in an unbounded volume conductor. Biol Cybern 61:205–210

Stephanova DI, Daskalova M, Alexandrov AS (2005) Differences in potentials and excitability properties in simulated cases of demyelinating neuropathies. Part I. Clin Neurophysiol 116:1153–1158

Stephanova DI, Daskalova M, Alexandrov AS (2006a) Differences in membrane properties in simulated cases of demyelinating neuropathies. Internodal focal demyelinations without conduction block. J Biol Phys 32:61–71

Stephanova DI, Daskalova M, Alexandrov AS (2006b) Differences in membrane properties in simulated cases of demyelinating neuropathies. Internodal focal demyelinations with conduction block. J Biol Phys 32:129–144

Stephanova DI, Alexandrov AS, Kossev A, Christova L (2007) Simulating focal demyelinating neuropathies: membrane property abnormalities. Biol Cybern 96:195–208

Sung JY, Kuwabara S, Kaji R, Ogawara K, Mori M, Kanai K, Nodera H, Hattori T, Bostock H (2004) Threshold electrotonus in chronic inflammatory demyelinating polyneuropathy: correlation with clinical profiles. Muscle Nerve 29:28–37

Weiss G (1901) Sur la possibilité de rendre comparables entre eux les appareils servant à l'excitation électrique. Arch Ital Biol 35:413–446